

A&amp;A manuscript no.

(will be inserted by hand later)

Your thesaurus codes are:

03(11.09.1 M31; 11.19.4; 11.08.1; 08.11.1; 03.20.7; 03.13.5)

ASTRONOMY  
AND  
ASTROPHYSICS  
28.8.2021

# Velocity dispersions and mass-to-light ratios for 9 globular clusters in M31

P. Dubath<sup>1,2</sup>, Carl J. Grillmair<sup>3</sup><sup>1</sup> Observatoire de Genève, ch. des Maillettes 51, CH-1290 Sauverny, Switzerland<sup>2</sup> INTEGRAL Science Data Centre, ch. d'Écogia 16, CH-1290 Versoix, Switzerland<sup>3</sup> Jet Propulsion Laboratory, 4800 Oak Grove Drive, Mail Stop 179-225, Pasadena, CA 91109

Received , accepted

**Abstract.** We present internal velocity dispersion determinations from high-resolution spectroscopic observations of a sample of nine globular clusters in M31. Comprehensive numerical simulations are used to show that the typical uncertainty of our velocity dispersion measurements is  $\sim 5\%$ . Using these new velocity dispersions together with structural parameters derived from HST observations, we estimate the  $M/L_V$  ratios of these clusters and find that they are typical of those measured for Galactic clusters. We show relations between velocity dispersion, luminosity and physical scales for globular clusters belonging to the Galaxy, the Magellanic clouds, Fornax, M31, and Centaurus A. The mean relations and the degree of scatter are similar in all galaxies. This reveals remarkable similarities, in term of structure and  $M/L_V$  ratio, between the globular clusters belonging to these different galaxies. We briefly discuss the possible use of individual globular clusters as extragalactic distance indicators.

**Key words:** Galaxies: individual: M31 – Galaxies: star clusters – Galaxies: halos – Stars: kinematics – Techniques: radial velocities – Methods: observational

## 1. Introduction

Valuable information about globular clusters and galaxy formation can be obtained by investigating the extent to which the properties of globular clusters belonging to different galaxies are similar. For example, differences in initial mass function during cluster formation and/or in subsequent cluster dynamical evolution, which may both depend on galactic environment, would translate into differences in present-day stellar content. The globular cluster stellar content can be characterized by the mass-to-light

( $M/L$ ) ratio, which can now be determined for relatively remote globular clusters.

Collecting all the available data from the literature, Pryor & Meylan (1993) derive  $M/L_V$  ratios for 56 Galactic globular clusters using King-Michie dynamical models. They obtain *global*  $M/L_V$  ratios ranging from about 1 to 5 with a mean of 2.3 (in solar units), and found no significant correlations (apart from a possible weak one between  $M/L_V$  and cluster mass) between the *global*  $M/L_V$  ratios and other parameters such as metallicity, concentration, half-mass relaxation time, or distance from either the Galactic center or the Galactic plane.  $M/L_V$  ratios similar to those obtained for Galactic clusters have been obtained in studies of globular clusters belonging to the Magellanic clouds (Dubath et al. 1996b) and to the Fornax dwarf spheroidal galaxy (Dubath et al. 1992).

Another way of investigating globular cluster similarities, in terms of structure and  $M/L_V$  ratio, is to look at the correlations between velocity dispersion, luminosity and a physical size scale. These correlations, which are analogous to the fundamental plane correlations for elliptical galaxies, have already been discussed for Galactic clusters by several authors (e.g., Meylan & Mayor 1986, Paturel & Garnier 1992, Djorgovski & Meylan 1994, Djorgovski 1995). The tight correlation between the velocity dispersion, the core radius and the central surface brightness obtained for Galactic clusters (Djorgovski 1995) is consistent with expectations from the Virial theorem assuming that Galactic globular cluster cores have a universal and constant  $M/L_V$  ratio to within the measurement errors.

Because of its relative proximity and large size, the M31 globular cluster system is an obvious target for the study of extragalactic clusters. Previous studies of various aspects of the M31 globular cluster system have been reviewed by Fusi Pecci et al. (1993), Huchra (1993), Tripicco (1993), and Cohen (1993). The only velocity-dispersion determinations of M31 clusters published so far are by Peterson (1988). Corresponding  $M/L_V$  ratio estimates are

given for two clusters and are found to be similar to those typically obtained for Galactic clusters. A limitation in this work, however, arises from the difficulty of measuring M31 cluster structural parameters from the ground. In M31 the angular sizes of core and half-light radii are typically  $\sim 0''.2$  and  $\sim 1''$ , respectively.

In this work, we present new velocity dispersion and  $M/L_V$  ratio determinations for a sample of M31 globular clusters, for which structural parameters derived from HST observations are available in the literature. The  $M/L_V$  ratio estimates are based on simple relations derived from the Virial theorem and from King models. Our velocity dispersion estimates are also key observational constraints for more detailed dynamical analyses, e.g., based on Fokker-Plank or King-Michie multi-mass models, which are beyond the scope of this paper.

The spectroscopic observations and the data reduction are presented in Sect. 2. Numerical simulations used for deriving velocity dispersions from the integrated-light spectra and the corresponding results are described in Sect. 3. Section 4 discusses the structural parameters, and  $M/L_V$  estimates are given in Sect. 5. The relations between velocity dispersion, luminosity and different physical scales are discussed in Sect. 6 for our M31 cluster sample together with samples of clusters belonging to the Galaxy, the Magellanic clouds, the Fornax dwarf spheroidal galaxy, and Centarus A. We summarize our findings in Sect. 7.

## 2. Observations and Data Reductions

We obtained 12 high-resolution integrated-light spectra of 10 globular clusters belonging to M31. The observations were made September 9-11, 1994 (see Table 1), with the Hamilton echelle spectrograph (Vogt 1987) operated at the coudé focus of the 3-m Shane telescope of the Lick Observatory. The detector was a thinned, backside-illuminated TI CCD, with  $800 \times 800$  pixels of  $15 \times 15 \mu\text{m}$  each, and with a readout noise of about 6 electrons.

During the first night, a relatively wide entrance slit of  $2''.0 \times 5''.0$  was used to match poor seeing conditions. A slit of  $1''.5 \times 5''.0$  was used during the second and the third nights. As a consequence, the instrumental resolution, as estimated from the FWHM of the emission lines of thorium calibration spectra, was slightly lower during the first night ( $31\,000$  or  $9.7 \text{ km s}^{-1}$ ) than during the second and the third ones ( $35\,000$  or  $8.6 \text{ km s}^{-1}$ ). Both slits used have widths larger than the apparent half-light radii (see Table 2) of all our clusters.

Table 1 gives the date of the observations, the exposure time ( $T_{\text{exp}}$ ) and the signal-to-noise (S/N) ratio of the cluster spectra. During each observing night, many radial velocity standard stars were also measured. Spectra of a thorium-argon lamp were taken 6-8 times through each of the three nights.

The spectra were reduced with INTER - TACOS, a new software package developed in Geneva by D. Queloz and L. Weber. The first-night spectra contain 50 useful orders ranging from  $4800$  to  $8300 \text{ \AA}$ , and those obtained the second and third night contain 49 orders ranging from  $4600$  to  $7500 \text{ \AA}$ . The different orders do not overlap, i.e., the echelle spectra exhibit holes in the wavelength coverage. The orders are never rebinned, nor merged together.

The shifts in velocity between the different thorium-argon lamp spectra taken during one particular night are always smaller than  $1 \text{ km s}^{-1}$ . However, a velocity shift as large as  $5 \text{ km s}^{-1}$  is observed between the second and the third nights. As a first step, for each night, one wavelength solution is computed from a thorium-argon spectrum, and applied to all the spectra taken during that particular night. The cluster spectra also contain numerous strong night-sky OH and O2 emission lines, because of the long exposure time on relatively faint objects. The residual velocity zero-point shift of each globular cluster spectrum is then derived by measuring<sup>1</sup> the mean shift (in velocity) of the emission lines compared to their accurate rest wavelengths (taken from Osterbrock et al. 1996). As a second step of the wavelength calibration, all the *globular cluster* spectra are corrected according to these velocity zero-point shifts.

The reduced spectra are cross-correlated with an optimized numerical mask, used as a template (see Dubath et al. 1990 for the details of the cross-correlation technique). In short, our template contains lower and upper wavelength limits for each line from a selected sample of narrow spectral lines. For a particular radial velocity, the value of the cross-correlation function (CCF) is given by the sum, over all spectral lines, of the integral of the considered spectrum within the lower and the upper line limits shifted according to the given velocity. The CCF is thus built step by step over the velocity range of interest. The CCF is not affected by the fact that the spectra are composed of a succession of independent orders, with holes in the wavelength coverage. The CCF is a kind of mean spectral line over the approximately 1400 useful lines spread over the spectral ranges of the different orders. The lower and upper limits of the lines are computed from a mix of observed and theoretical high-resolution spectra of K2 giants, in such a way as to optimize the CCF (see Dubath et al. 1996a).

When the number of considered lines is large enough ( $>$  several hundreds), this cross-correlation technique produces a CCF which is nearly a perfect Gaussian. A Gaussian function is fitted to each derived CCF in order to determine three physical quantities: (1) the location of the minimum equal to the radial velocity  $V_r$ , (2) its depth

<sup>1</sup> The measurement of the mean velocity shift of the night-sky emission lines is achieved by cross-correlating the observed spectrum with a template constructed using the rest wavelengths of the emission lines

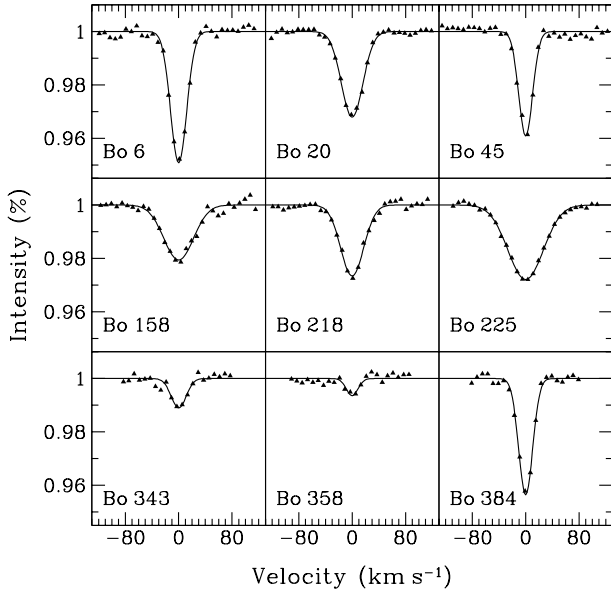


**Fig. 1.** Cross-correlation functions (CCFs) of the M31 globular cluster spectra. The dots represent the CCFs themselves, and the continuous lines represent the fitted Gaussians. Cluster designations are from Battistini et al. (1980).

$D$ , and (3) its standard deviation  $\sigma_{\text{CCF}}$ , related to line broadening mechanisms.

Figure 1 displays the CCFs of the integrated-light spectra obtained for the M31 globular clusters in our sample.

We have a total of 32 measurements of 11 standard stars, mostly giant stars of spectral type G8 to K4, collected during the same observing run. The comparison of the standard-star radial velocities with reference values provided by CORAVEL measurements (Mayor, private communication) shows that the instrumental radial velocity accuracy is of order  $0.5 \text{ km s}^{-1}$  and that the zero-point shift between the two datasets is not significant. In the case of the M31 clusters, the accuracy of the radial velocity zero-point is very probably even better owing to our use of the night-sky emission lines to calibrate the zero point of each cluster spectrum.

The mean value of the widths ( $\sigma_{\text{CCF}}$ ) of the CCFs obtained for our sample of standard stars is  $5.8 \pm 0.3 \text{ km s}^{-1}$  for the first night, and  $5.5 \pm 0.2$  for the two others. This difference is the direct consequence of the different slit widths used. We see no dependence of the CCF width on spectral type over the range considered here (G8 to K4). We also know that the CCF width does not depend on the star metallicity from previous measurements of a large number of various types of metal-deficient stars (see Fig. 6 of Dubath et al. 1996a).

### 3. Velocity dispersions from integrated-light spectra

The *projected* velocity dispersions can be derived from the broadening of the cluster CCFs. This broadening results from the Doppler line broadening present in the integrated-light spectra because of the random spatial motions of the stars. Since the spectrograph slit used is large compared to the the M31 globular clusters apparent size, a very large number of stars contributes significantly to the integrated light. Quantitatively, recent numerical simulations (Dubath et al. 1994, 1996a) show that statistical errors, which can be very important for integrated-light measurements of some Galactic globular clusters because of the dominance of a few bright stars, are negligible in the present case. An integrated light spectrum of an M31 globular cluster is well approximated by the convolution of the spectrum of a typical globular cluster star with the projected velocity distribution.

Since the CCF is a kind of mean spectral line, the above property also hold for CCFs. The CCF of an integrated-light spectrum of a globular cluster is the convolution of the CCF of the spectrum of a typical globular cluster star by the projected velocity distribution. Since the CCFs have a Gaussian shape, an estimate of the projected velocity dispersion  $\sigma_p$  in the integration area of a globular cluster is given by the quadratic difference,

$$\sigma_p^2 = \sigma_{\text{CCF}}^2(\text{cluster}) - \sigma_{\text{ref}}^2, \quad (1)$$

where  $\sigma_{\text{CCF}}$  is the width of the Gaussian fitted to the cluster CCF and  $\sigma_{\text{ref}}$  is the average width of the  $\sigma_{\text{CCF}}$  obtained for a sample of standard stars, as representative as possible of the cluster stars which contribute most to the integrated light.

We do not use this formula directly in the present study. In order to derive the cluster projected velocity dispersion, we carry out a large number of numerical simulations. The results of these simulations confirm, however, the validity of Eq. 1 (see Sect. 3.1.1).

#### 3.1. Numerical Simulations

In order to simulate the integrated-light spectrum and the CCF obtained for globular cluster, we proceed in several steps. In the first row of Fig. 2, the integrated-light spectrum (left) and the CCF (right) obtained for the cluster Bo 218 are displayed. Corresponding simulation results are displayed in the last row, while the intermediate steps of the simulation are illustrated in the middle row of this figure.

1. The simulation input parameter is the cluster velocity dispersion ( $\sigma_{\text{in}}$ ). The simulation starts with a high signal-to-noise spectrum of a standard star of appropriate spectral type, e.g., a K2 giant. To simulate the Doppler line broadening, this spectrum is convolved with a Gaussian function of standard deviation equal to the input ve-

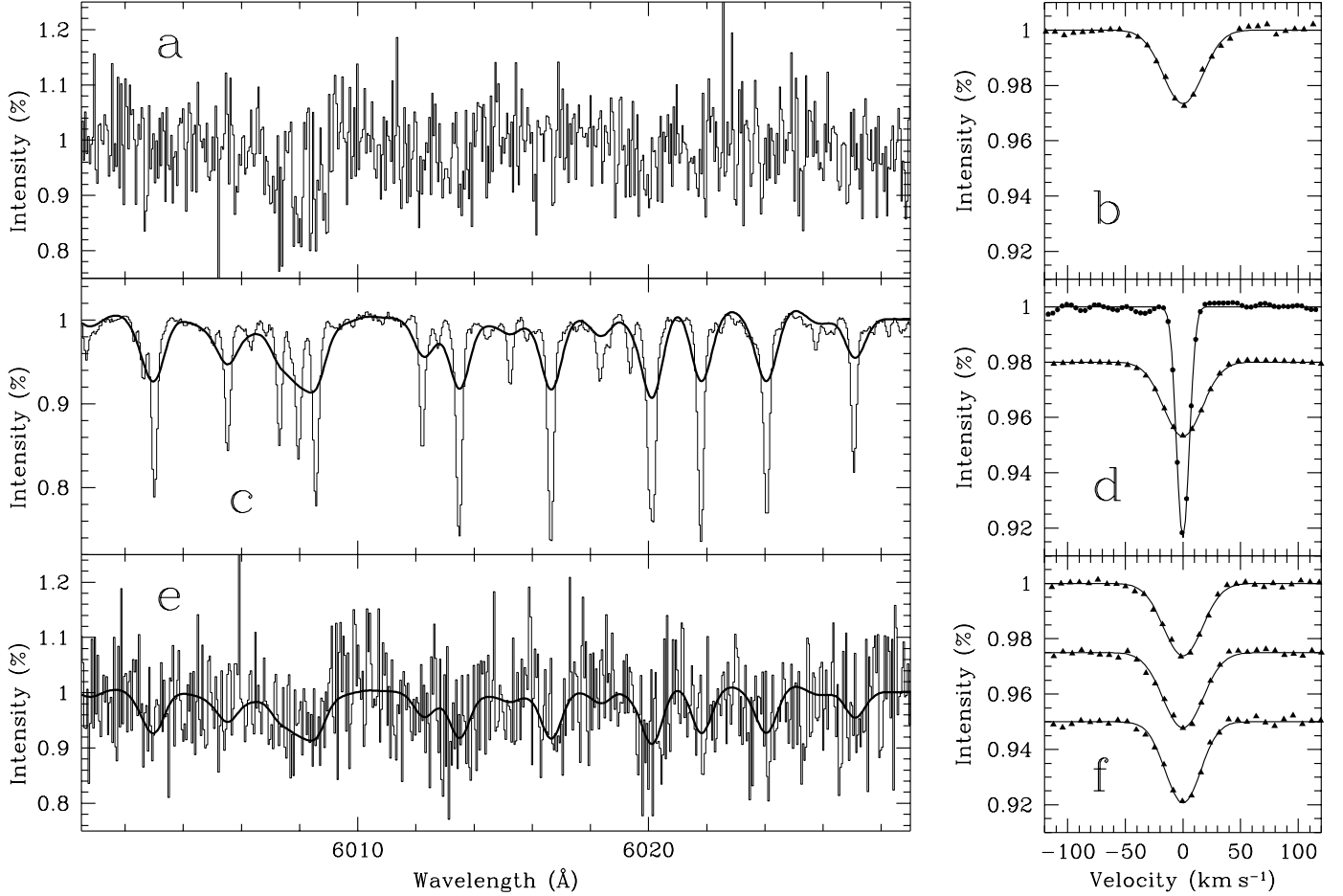


**Fig. 2.** Illustration of the numerical simulations in the case of the cluster Bo 218. This figure displays: (a) the *observed* integrated-light spectrum of the cluster; (b) its cross-correlation function (CCF); (c) the original and the convolved standard-star template spectrum; (d) their corresponding CCFs, one arbitrarily shifted for the purpose of display; (e) the convolved template spectrum (again) and one example of this spectrum with additional noise, simulating the *observed* cluster spectrum (panel a); and (f) three examples of CCFs of noisy convolved spectra taken at random and arbitrarily shifted, simulating the cluster CCF (panel b). This figure shows only a tiny fraction of the spectra ( $\sim 1/50$  of their total wavelength range).

locity dispersion  $\sigma_{\text{in}}$ . A portion of the standard-star spectrum, before and after convolution, is shown in the panel (c) of Fig. 2.

2. In general, the spectral lines of the convolved standard-star spectrum do not have the same depths as those of a given cluster spectrum, mainly because of possible metallicity difference. The next step is thus to adjust the depth of the standard-star spectral lines. This is done by scaling the convolved standard-star spectrum so that its CCF is of the same depth as the cluster CCF. (With our cross-correlation technique, there is a clear relationship between the average depth of the spectral lines of a spectrum and the depth of the spectrum CCF). In Fig. 2 for example, the spectra and the CCFs displayed in the middle row are linearly scaled so that the convolved spectrum CCF (the broad CCF in panel d) be of the same depth as the cluster CCF (in panel b). A noiseless tem-

plate of a cluster spectrum – for one particular velocity dispersion  $\sigma_{\text{in}}$  – results from the second step.

3. Random noise is added to this template spectrum to simulate the photon counting and CCD readout noises of observed cluster spectra. A portion of the template spectrum for Bo 218 (c) and of one example of simulated noisy spectrum are displayed in panel (e) of Fig. 2. We then cross-correlate the simulated noisy spectrum and derive the radial velocity ( $V_r$ ) and the sigma ( $\sigma_{\text{CCF}}$ ) of the resulting CCF. This third step is repeated a large number of times (100 to 150 times) to observe the influence of the noise on  $V_r$  and  $\sigma_{\text{CCF}}$ . Panel (f) of Fig. 2 shows three examples of simulated CCFs taken at random. The comparison of the upper and the lower panels of this figure shows how well our simulations reproduce the integrated-light spectrum and the CCF obtained for Bo 218.

In order to derive the best estimates of the projected velocity dispersion ( $\sigma_p$ ) in the clusters, we proceed as fol-

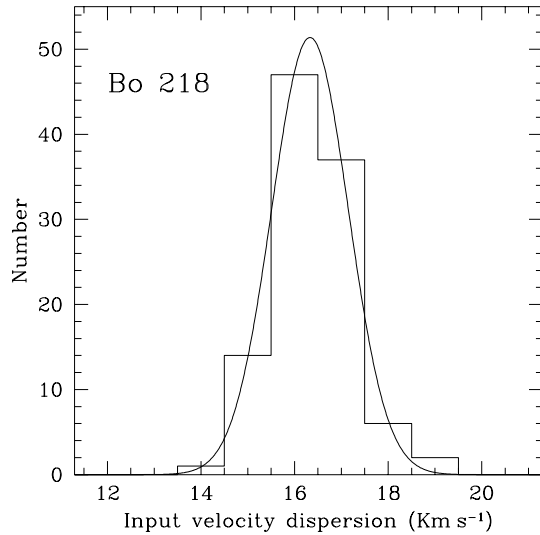


**Fig. 3.** Distribution of the number of time that the simulations produce a CCF consistent – in terms of width – with the observed CCF as a function of the input velocity dispersion ( $\sigma_{\text{in}}$ ), in the case of Bo 218. For each  $\sigma_{\text{in}}$ , 100 simulations are considered. The continuous line represents a Gaussian fitted to the distribution.

lows. For each cluster, a set of different input velocity dispersions ( $\sigma_{\text{in}}$ ), varying by step of 0.5 or 1  $\text{km s}^{-1}$  around the expected cluster “true” velocity dispersion (first evaluated with Eq. 1) are considered. For each  $\sigma_{\text{in}}$ , 100 or 150 simulations are carried out and the relative number of times that the width of the simulated CCFs is consistent with the width of the observed CCF is reported. Consistent means here that the sigma of the simulated CCF must be within  $\pm 0.2\text{--}0.5 \text{ km s}^{-1}$  (depending on the different cases) of the sigma of the observed CCF. Figure 3 shows, in the case of Bo 218, the distribution of these numbers as a function of the input velocity dispersions ( $\sigma_{\text{in}}$ ) of the simulations. This distribution is a kind of probability distribution; the best estimate of the “true” cluster velocity dispersion is given by the  $\sigma_{\text{in}}$  which leads most often, through the simulations, to a CCF consistent with the observed one. For example, among 100 simulations carried out with  $\sigma_{\text{in}} = 16 \text{ km s}^{-1}$ , 47 have a width consistent with the width of the observed CCF obtained for Bo 218, while none of the 100 simulations with  $\sigma_{\text{in}} = 13 \text{ km s}^{-1}$  is successful in reproducing the observed CCF.

A similar distribution is derived for each cluster, and a Gaussian is fitted to each of them. The resulting means and sigmas, which provide the most probable cluster velocity dispersions ( $\sigma_p$ ) and their uncertainties, are given in column (11) of Table 1.

### 3.1.1. Generalization

This section presents a generalization of the simulation results (which can be skipped by less concerned readers).

For each of the 9 clusters, simulations are carried out for a set of input velocity dispersions ( $\sigma_{\text{in}}$ ). In the simulations, a particular cluster is characterized by the spectrum S/N ratio and by the depth ( $D$ ) of the cluster CCF. Therefore in general, the input parameters are the spectrum S/N, the CCF depth  $D$ , and the input velocity dispersion  $\sigma_{\text{in}}$ . For each set of input parameters, 100 to 150 simulated CCFs are computed, and distributions of the resulting radial velocities and CCF sigmas are thus produced. The standard deviations of these distributions –  $\varepsilon(V_r)$  for the radial velocities and  $\varepsilon(\sigma_{\text{CCF}})$  for the sigmas – provide estimates of the uncertainties due to the spectrum noise. The following formula,

$$\varepsilon = \frac{C}{S/N D} (1 + \alpha \sigma_{\text{in}}) \quad (2)$$

where  $C$  and  $\alpha$  are two constants, is fitted to the results of the simulations. With  $C = 0.09$  and  $\alpha = 0.06$ , this equation gives in  $\text{km s}^{-1}$ , (1)  $\varepsilon(V_r)$  with an accuracy of order of 10%, and (2)  $\varepsilon(\sigma_{\text{CCF}})$  with an accuracy of about 20%. It can then be used to estimate the uncertainties due to the spectrum noise in a more general way, for any set of parameters S/N,  $D$ , and  $\sigma_{\text{in}}$ . Equation 2 is a generalization of Eq. (3) of Dubath et al. (1990) to broad CCFs. The constant  $C$  is lower in the present paper than in this previous study because the larger wavelength range, and consequently larger number of spectral lines, taken into account in the cross-correlation process ( $C$  scales roughly with the square root of the number of lines).

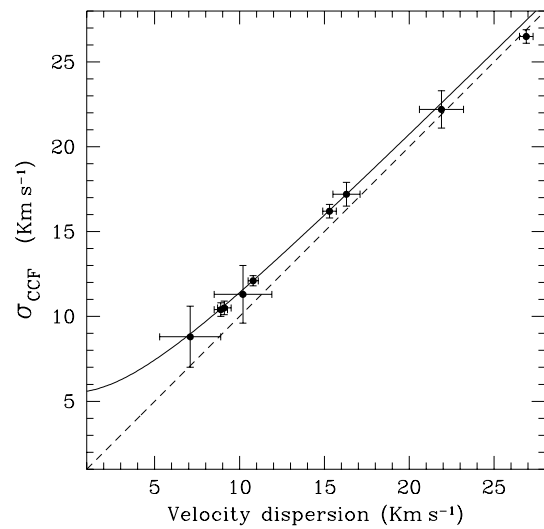


**Fig. 4.** Relation between the sigmas ( $\sigma_{\text{CCF}}$ ) of the observed CCFs and the best estimates of the velocity dispersions ( $\sigma_p$ ) resulting from the simulations. Each point displays the result for one of the 9 M31 clusters. The continuous line represents Eq. (1), whose validity is thus confirmed by the results of the simulations.

Figure 4 displays, for each cluster, the sigma ( $\sigma_{\text{CCF}}$ ) of the CCFs of the observed spectrum as a function of the corresponding estimates of the velocity dispersion ( $\sigma_p$ ) resulting from the simulations. Eq. (1) is illustrated in this figure by the continuous line, and the good agreement with the simulation results indicates that this equation is a valid model.

### 3.2. Results

For each observation, Table 1 lists the cluster identification from Battistini et al. (1980) in column (1), and from Sargent et al. (1977) in column (2), the cluster apparent V magnitude in column (3), the cluster [Fe/H] in column (4), the date of the observation in column (5), the exposure time in column (6), the signal-to-noise ratio of the integrated-light spectrum in column (7), the heliocentric radial velocity in column (8), the depth of the CCF in column (9), the sigma of the CCF in column (10), and the projected velocity dispersion in column (11). The cluster apparent V magnitudes are taken from Battistini et al. (1987), and [Fe/H] are taken from Huchra et al. (1991).

The radial velocity errors given in column (8) of Table 1 are computed using Eq. (2). This equation provides an estimate of the error due to the spectrum noise (photon counting and CCD readout noises) but does not take into account the uncertainty of the zero-point corrections computed from measurements of the night-sky emission lines. Consequently, the radial velocity errors smaller than  $\sim 0.3 \text{ km s}^{-1}$  are probably underestimated. The  $\sigma_{\text{CCF}}$  errors given in column (10) of Table 1 are the square root of the quadratic sum of the errors due to the noise (estimated using Eq. (2)), and of an instrumental error of  $0.25 \text{ km s}^{-1}$ , derived from standard-star measurements.

Two cluster spectra are too noisy to provide useful velocity dispersion estimate. The CCF obtained for Bo 147 is as narrow as the CCFs obtained for individual standard stars, and much narrower than the value expected from its absolute magnitude. Consequently, Bo 147 is almost certainly a foreground star.

### 4. Structural parameters

M31 is at a distance where the core radii of typical globular clusters are considerably smaller in angular size than the typical, ground-based seeing disk. This makes measurements of  $r_c$  difficult, as attested to by the large range of values obtained by different authors for the same clusters. Fortunately, six of the clusters in our sample have recently been observed with the Hubble Space Telescope (HST), and accurate values of  $r_c$  have been published (Fusi-Pecchi et al. 1994 [Bo218, 384]; Grillmair et al. 1996 [Bo6, 45, 343, 358]). The values obtained span a large range but are typical for the brighter globulars in our own Galaxy. For the remaining 3 clusters in Table 1, we use the ground-based measurements of Battistini et al. (1982) and Crampton

et al. (1985). For two clusters (Bo6, 45) common to all three samples, the agreement between the ground-based values and those measured by Grillmair et al. is typically quite good, with the worst cases differing by no more than 30%.

The surface density profiles of these clusters have also been difficult to characterize from the ground owing the very low surface brightness relative to the M31 background and the inability to resolve individual stars. However with the advent of HST we now know that globular clusters in M31 are structurally similar to those found in our own Galaxy. These clusters can generally be characterized by King models, though departures from King models in the form of collapsed cores (Bo343, Bendinelli et al. 1993; Grillmair et al. 1996) and tidal tails (Bo6, 343, 358, Grillmair et al. 1996) have also been found. In all respects, it seems that globular clusters in M31 as a group are of the same breed as the clusters belonging to our own Galaxy.

For the clusters observed by Grillmair et al. (1996), we have determined the half-light radii  $r_{hp}$  (the radii within which half the total light of the clusters is contained in projection) by integrating over King models with appropriate core radii and concentration parameters ( $c = \log r_t / r_c$ ). For the 2 clusters observed by Fusi Pecchi et al. (1994) we have used their core and half-light radii and integrated over a grid of King models to infer the corresponding concentration parameter. For the three clusters for which we have only ground-based measurements of  $r_c$ , we follow Battistini et al. (1982) in assuming a uniform value of  $r_t = 60 \text{ pc}$ . Our adopted values of  $r_c$  and  $r_{hp}$  are tabulated in Table 2. In all cases, the published values of  $r_c$  have been scaled in accordance with our adopted distance to M31 of 770 kpc (Ajhar et al. 1996).

### 5. Mass-to-light ratios

If we assume that the clusters are reasonably well represented by King models then, following Queloz et al. (1995), we can compute the total mass using

$$M_{cl} = \frac{9}{2\pi G} \frac{\mu r_c \sigma_p^2(0)}{\alpha p}. \quad (3)$$

Values of  $\mu$ ,  $\alpha$ , and  $p$  have been tabulated for a range of concentration parameters by King (1966) and Peterson & King (1975).

The  $\sigma_p(0)$  in Eq. 3 refers to the *central* velocity dispersion of the cluster. Given the small angular size of the clusters and our use of 1.5 and 2.0 arcsecond-wide slits, it is clear that our dispersion measurements will have been influenced by light from moderately large radii. We tested the effect of our slit-widths on the measured velocity dispersions by integrating luminosity-weighted, King model velocity dispersion profiles over the area subtended by our slit. We found that, over a large range in  $c$ , and for both slit-widths used, the measured velocity dispersion would

**Table 1.** Radial velocities and velocity dispersions of M31 globular clusters

Cluster number		$m_V$	[Fe/H]	Date	Texp	S/N	$V_r$	$D$	$\sigma_{\text{CCF}}$	$\sigma_p$
				94 Sept.	(min)		( $\text{km s}^{-1}$ )	(%)	( $\text{km s}^{-1}$ )	( $\text{km s}^{-1}$ )
(1)	(2)	(3)	(4)	(5)	(6)	(7)	(8)	(9)	(10)	(11)
6	58	15.8	-0.57	9	100	13	-236.9±0.2	4.9	12.1±0.3	10.6±0.4
20	73	14.6	-1.07	11	100	18	-350.8±0.3	3.2	16.2±0.4	15.3±0.5
45	108	15.8	-0.94	9	85	11	-425.1±0.3	3.9	10.4±0.4	8.7±0.5
147	199	15.5	-0.24	11	80	26	-50.7±0.1	7.3	6.0±0.3	star?
158	213	14.5	-1.08	10	50	10	-186.5±1.0	2.1	22.2±1.1	21.9±1.3
218	272	14.7	-1.18	11	50	11	-220.2±0.6	2.7	17.2±0.7	16.3±0.8
225	280	14.3	-0.70	9	120	31	-164.8±0.3	2.8	26.5±0.4	26.9±0.5
343	105	16.3	-1.49	11	100	8	-359.6±1.7	1.1	11.3±1.7	10.2±1.7
"	"	"	"	10	63	4	-357.5±4.0	0.7	7.7±4.1	...
358	219	15.1	-1.83	10	90	12	-315.1±1.8	0.6	8.8±1.8	7.1±1.8
"	"	"	"	9	50	6	-317.5±3.1	0.8	12.0±3.1	...
384	319	15.7	-0.66	11	100	10	-363.8±0.3	4.4	10.5±0.4	9.1±0.5

**Table 2.** Mass-Luminosity Ratios for M31 Globular Clusters

Cluster ID	$r_c$ pc	$r_{hp}$ pc	$c$	$M_V$	$M_{cl}$ $M_\odot$	$M_{cl}^{Virial}$ $M_\odot$	E(B-V)	$M/L_V$ $M_\odot/L_{\odot,V}$	$M/L_V^{Virial}$ $M_\odot/L_{\odot,V}$	
(1)	(2)	(3)	(4)	(5)	(6)	(7)	(8)	(9)	(10)	(11)
6	58	0.62	2.8	1.76	-9.0	$4.6 \times 10^5$	$7.3 \times 10^5$	0.11	1.4	2.2
20	73	1.18	4.7	1.71	-10.2	$1.7 \times 10^6$	$2.6 \times 10^6$	0.11	1.7	2.5
45	108	0.92	3.6	1.70	-9.0	$4.2 \times 10^5$	$6.3 \times 10^5$	0.12	1.2	1.8
158	213	1.54	5.0	1.59	-10.2	$3.8 \times 10^6$	$5.6 \times 10^6$	0.08	3.7	5.5
218	272	0.47	2.0	1.74	-10.0	$7.9 \times 10^5$	$1.2 \times 10^6$	0.09	0.9	1.4
225	280	1.42	4.9	1.63	-10.4	$5.5 \times 10^6$	$8.2 \times 10^6$	0.09	4.4	6.5
343	105	0.34	2.9	2.02	-8.3	$3.7 \times 10^5$	$7.0 \times 10^5$	0.06	2.1	4.0
358	219	1.82	4.7	1.46	-9.5	$4.0 \times 10^5$	$5.5 \times 10^5$	0.06	0.7	1.0
384	319	0.57	2.2	1.69	-8.9	$2.8 \times 10^5$	$4.3 \times 10^5$	0.06	0.9	1.4

be lower than the central velocity dispersion by about 5%. Hence, for the purposes of computing masses, we increased the measured dispersions in Table 1 accordingly. The resulting cluster masses we obtain using Eq. 3 are listed in column 7 of Table 2.

An alternative to the somewhat model-specific method used above is a straightforward application of the Virial theorem:

$$M_{cl} \simeq \frac{4\sigma_p^2 r_{hp}}{0.4G}, \quad (4)$$

where we have assumed an isotropic velocity distribution and  $r_{hp} \approx \frac{4}{3}r_h$  (Spitzer 1987), where  $r_h$  is the half-mass radius. The masses computed using this equation are given in column 8 of Table 2.

Owing to M31's low Galactic latitude, obscuration of the globular clusters by foreground Galactic dust varies significantly from one side of M31 to the other. Using the extinction maps of Burstein & Heiles (1982), E(B-V)

was estimated for each cluster and is given in column 9 of Table 2. Using the  $V$ -magnitudes given by Battistini et al. (1987), we adopt  $A_V = 3.2$  E(B-V) (DaCosta & Armandroff 1990), and  $(m - M_V) = 24.432$  to compute total cluster  $V$ -band luminosities. The corresponding values for  $M/L_V$  are given in column 10 and 11 of Table 2.

The  $M/L_V$  ratios given in Table 2 are remarkably similar to those typically found in Galactic globulars (Pryor & Meylan 1993). Bo158 and 225 might seem a trifle high, but we note that both these clusters have only ground-based measurements of  $r_c$ . It is entirely possible that these estimates of  $r_c$  suffer from incomplete removal of the effects of seeing and are consequently too high. The largest source of uncertainty in  $M/L_V$  is generally in the estimation of  $r_c$ , being of the order of 15% even for the HST-imaged clusters. Uncertainties in the magnitude estimates of Battistini et al., in our estimates of the local extinction, and in the velocity dispersion measurements contribute  $\leq 10\%$  each to the final uncertainty. Bo343 and 358 are exceptions

to this general rule, having reasonably well-measured core radii, but rather less well-determined velocity dispersions. The formally estimated uncertainties in  $M/L_V$  are  $\approx 20\%$  for those clusters observed with HST, and probably closer to 50% for those clusters imaged only from the ground.

Table 2 shows that the  $M/L_V$  ratios derived with Eq. 4 (column 11) are systematically  $\sim 50\%$  larger than those obtained with Eq. 3 (column 10). This gives a rough idea on how model dependent are our estimates.

## 6. Relation between velocity dispersion, luminosity, and a physical scale

Another way to investigate similarities among different globular cluster populations is to look at the relation between velocity dispersion, luminosity, and a physical size scale. In such a parameter space, systematic differences between two systems of globular clusters, in terms of structure or  $M/L$  ratio, would result in either different mean relations or in different degrees of scatter about a given relation. We do not attempt here to derive mean relations through bivariate fits (e.g. Djorgovski 1995) as they turn out to be rather unstable because of both the small number of data points as well as the weak correlation between the physical size parameter and the luminosity and velocity dispersion. Instead, we fit to the data the relations expected from the Virial theorem, or from the King models. Assuming a constant  $M/L_V$  ratio, the Virial Theorem predicts the relation

$$5 \log \sigma + 2.5 \log r_{hp} \sim -M_V \quad (5)$$

between the *global* velocity dispersion  $\sigma$ , the half-light radius  $r_{hp}$ , and the absolute visual magnitude  $M_V$ . Similarly, King models predict

$$5 \log \sigma_0 + 2.5 \log \mu r_c \sim -M_V, \quad (6)$$

where  $\sigma_0$  is the *central* velocity dispersion,  $\mu$  a dimensionless parameter which varies with cluster concentration  $c$ ,  $r_c$  the core radius, and  $M_V$  the absolute visual magnitude. Figure 5 shows the relations between  $5 \log \sigma$  vs.  $M_V$  (uppermost row of panels),  $5 \log \sigma + 2.5 \log r_h$  vs.  $M_V$  (second row), and  $5 \log \sigma + 2.5 \log \mu r_c$  vs.  $M_V$  (third row), for different data sets. For the Galactic clusters we use velocity dispersion measurements based on radial velocities of individual stars, taken from the compilation of Pryor and Meylan (1993). For the other clusters, we use velocity dispersions derived from integrated-light observations, taken from Dubath et al. (1996a) for 8 old Magellanic clusters, from Dubath et al. (1992) for 3 clusters belonging to the Fornax dwarf spheroidal galaxy, from the present study for 9 M31 clusters, and from Dubath (1994) for 10 Centaurus A clusters. The continuous lines represent the relation  $5 \log \sigma = Cst - M_V$  (uppermost row), and the relations (5) and (6), in the second and third rows respectively, with constants derived by fitting the *Galactic* cluster data. The

dashed lines show the relations obtained when central velocity dispersions (extrapolated for these clusters by Pryor and Meylan [1993] using King models) are considered instead of the *global* velocity dispersion.

It is worth mentioning that correlations resulting from bivariate fits do not differ much from the relations expected from the Virial theorem (Djorgovski 1995), and that Fig. 5 would look very similar if slightly different projections were used. The scatter of the data points probably results to a large extent from measurement errors, and it is quite remarkable that this scatter is of the same order in all panels of Fig. 5. The similarity of the different panels of Fig. 5 indicates both that there is no large systematic differences in globular cluster  $M/L_V$  ratios between one galaxy to another, and that measurement errors are comparable, and even smaller, for extragalactic clusters than for Galactic clusters.

In the first row of Fig. 5, we expect a higher degree of scatter since the physical scale of each cluster (which acts as a second parameter) is not taken into account. Notably, a few large-size/low-concentration Galactic clusters lie well below the other clusters in the upper left panel. The fact that similar large clusters are not present in our M31 and Cen A samples is due to a selection bias which favors brighter and generally more compact clusters. In any case, the relatively small spread of the data points around the straight lines in the uppermost panels points to an additional similarity in terms of physical size range between the clusters of these different galaxies, with the possible exception of the old Magellanic clusters. This is particularly interesting in the case of the Centaurus A clusters since these clusters are brighter than the Galactic ones, but their physical scales have not yet been measured.

For the old Magellanic clusters, the products  $\mu r_c$  are systematically *smaller* than the Galactic average. This can perfectly explain why the Magellanic clusters appear above the Galactic relation in the upper panel in Fig. 5, while the Magellanic and Galactic middle panels are similar. The lower panel is, however, rather puzzling. Unexpectedly, the data points all lie above the Galactic relation, as if the half-light radii used here and taken from van den Bergh (1994) were about 40% too large. This point is further discussed in another paper (Dubath et al. 1996b).

The two M31 clusters (Bo158 & 225) with large  $M/L_V$  ratio estimates from last section stand out above the Galactic relation in Fig. 5. As already pointed out, these clusters only have ground-based measurements of  $r_c$  which may be overestimates. The scatter of the other clusters is remarkably small compared to the scatter of Galactic clusters.

### 6.1. Individual globular clusters as extragalactic distance indicators?

As illustrated in Fig. 5, the absolute magnitude of an individual globular cluster can be derived from its velocity



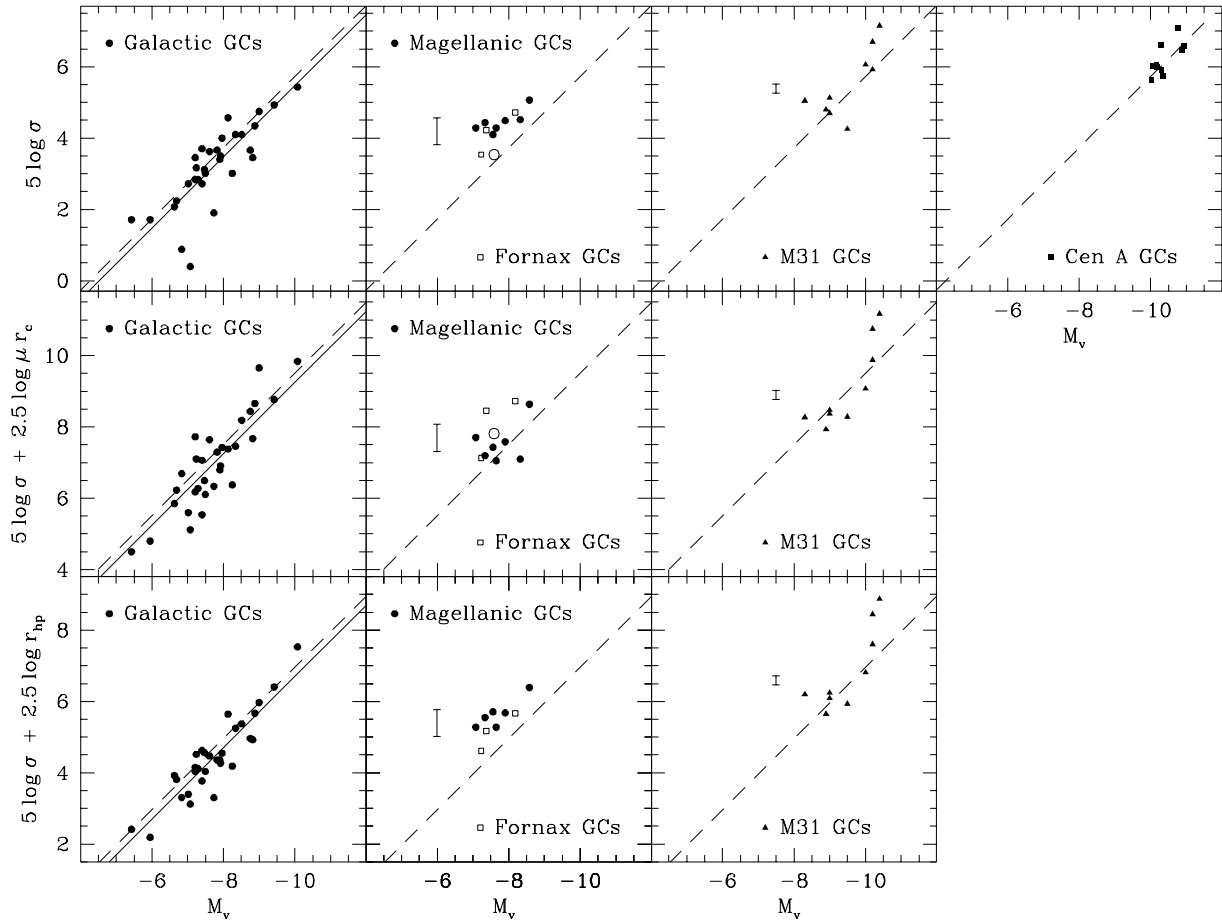


**Fig. 5.** Different projections of the fundamental plane for Galactic, old Magellanic, Fornax, M31, and Centaurus A globular clusters. Shown are the velocity dispersion  $\sigma_p$  (uppermost row of panels), and combinations of  $\sigma_p$  with physical scales – the product of the dimensionless mass  $\mu$  and the core radius  $r_c$  (second row) and half-light radius  $r_{hp}$  (third row) – as a function of the absolute visual magnitude  $M_V$ . The straight lines are derived by fitting the relations derived from King models (Eq. 6) or the Virial Theorem (Eq. 5) to the *Galactic* clusters data (left panels) only, using the *global* (continuous lines) or the *central* (dashed lines) velocity dispersions. Consequently, the different dashed lines in each row are identical and are displayed for comparison with the data. The circle represents NGC 121, the only SMC cluster. The error-bars represent  $7 \pm 1.2 \text{ km s}^{-1}$  in the case of Magellanic clusters and  $12 \pm 0.7 \text{ km s}^{-1}$  in the case of M31 clusters, and illustrate the typical errors of our  $\sigma_p$  measurements

dispersion and physical scale with an accuracy of  $\sim 0.5$  magnitude. For a given parent galaxy, providing there is no systematic differences in  $M/L_V$ , an accurate distance modulus can in principle be computed using the mean distance modulus of a moderate number (10 – 20) of its associated globular clusters. In other word, plotting apparent instead of absolute magnitude in Fig. 5, the difference between the distance moduli of two parent galaxies is given by the horizontal shift required to bring the two (dereddened) data sets in agreement. Combining the capabilities of the HST and of 10-m class, ground-based telescopes, this method could be applied for galaxies out as far as the Virgo cluster.

## 7. Summary

In this paper, we present projected velocity dispersion measurements from integrated-light spectra for a sample of 9 M31 globular clusters. By means of comprehensive numerical simulations, we show that the typical relative uncertainty of our measurements is  $\sim 5\%$ . Because of the relatively large distance of M31 and the aperture angular size used our integrated-light observations sample a large fraction of these very bright clusters. Consequently, statistical uncertainties due to small samples of bright dominant stars which can affect integrated-light measurements of nearby Galactic clusters are completely negligible. This is confirmed by numerical simulations presented in Dubath et al. (1996a). Paradoxically, it is in some respects easier to measure the *global* velocity dispersion of a M31 cluster than that of a Galactic clusters. For the brightest

M31 clusters, reliable velocity dispersions can be measured with a 3-m-class telescope using single exposures of order one hour long.

Previous velocity dispersion measurements are available from Peterson (1988) for 3 of our clusters. The agreement is good for the cluster Bo20, while we obtain significantly lower and more accurate values for Bo158 and 225.

Combining the new velocity dispersions with structural parameters, we compute the cluster  $M/L_V$  ratios using relations derived from King models and the Virial theorem. These  $M/L_V$  ratios appear remarkably similar to those found for Galactic clusters (see e.g., Pryor & Meylan 1993). Two clusters (Bo158 & 225) having only ground-based measurements of  $r_c$  have  $M/L_V$  ratio estimates somewhat above the range of Galactic values. It is entirely possible that these estimates of  $r_c$  suffer from incomplete removal of the effects of seeing and are consequently too high.

Another way to investigate similarities of globular clusters located in different parent galaxies is to look at the relation between velocity dispersion, luminosity and a physical scale (Fig 5). Using additional data from previous papers, we find remarkable similarities, in terms of  $M/L_V$  ratios and structures, between the globular clusters located in our Galaxy, the Magellanic clouds, the Fornax dwarf spheroidal, M31, and Centaurus A. It is worth emphasizing that our samples include some of the brightest M31 and Centaurus A clusters, which are both brighter and more massive than any Galactic cluster, as expected because of the larger number of clusters in both these galaxies.

Our M31 cluster sample is not large enough to investigate possible correlations between the  $M/L_V$  ratio estimates and other cluster parameters. Only a weak correlation is observed with Galactic data (Pryor & Meylan 1993), and it is possible that the variations of the current  $M/L_V$  estimates from one cluster to another result to a large extent from measurement errors.

*Acknowledgements.* P.D. acknowledge support through a grant from the Swiss National Science Foundation. P.D. warmly thanks Graeme Smith for providing free use of his workstation during a postdoctoral stay at the Lick Observatory.

## References

- Ajhar, E.A., Grillmair, C.J., Lauer, T.R., Baum, W.A., Faber, S.M., Holtzman, J.A., Lynds, C.R., & O'Neil, E.J. Jr. 1996, *AJ*, 111, 1110
- Battistini, P., Bònoli, F., Braccisi, A., Federici, L., Fusi Pecci, F., Marano, B., & Borngen, F. 1987, *A&AS*, 67, 447
- Battistini, P., Bònoli, F., Braccisi, A., Fusi Pecci, F., Malagnini, M. & Marano, B. 1980, *A&AS*, 42, 357
- Battistini, P., Bònoli, F., Buonanno, R., Corsi, C.E., & Fusi Pecci, F., 1982, *A&A*, 113, 39
- Bendinelli, O., Cacciari, C., Djorgovski, S., Federici, L., Ferraro, F.R., Fusi Pecci, F., Parmeggiani, G., Weir, N., & Zavatti, F. 1993, *ApJ Letters*, 409, L17
- Burstein, D., & Heiles, C. 1982, *AJ*, 87, 1165
- Cohen, J.G. 1993 in *ASP Conf. Ser.*, Vol. 48, *The Globular Cluster – Galaxy Connection*, G. Smith & J. Brodie (San Francisco: ASP), 438
- Crampton, D., Schade, D.J., Chayer, P., & Cowley, A.P. 1985, *ApJ*, 288, 494
- DaCosta, G.S., & Armandroff, T.E. 1990, *AJ*, 100, 162
- Djorgovski, S., & Meylan, G. 1994, *AJ*, 108, 1292
- Djorgovski, S. 1995, *ApJL*, 438, L29
- Dubath, P. 1994, *BAAS*, 185, 5203
- Dubath, P., Meylan, G., Mayor, M., & Magain, P. 1990, *A&A*, 239, 142
- Dubath, P., Meylan, G., & Mayor, M. 1992, *ApJ*, 400, 510
- Dubath, P., Meylan, G., & Mayor, M. 1994, *ApJ*, 426, 192
- Dubath, P., Meylan, G., & Mayor, M. 1996a, *A&A*, in press
- Dubath, P., Meylan, G., & Mayor, M. 1996b, *A&A*, submitted
- Fusi Pecci, F., Cacciari, C., Federici, L., & Pasquali, A. 1993, in *ASP Conf. Ser.*, Vol. 48, *The Globular Cluster – Galaxy Connection*, G. Smith & J. Brodie (San Francisco: ASP), 410
- Fusi Pecci, F., Battistini, P., Bendinelli, O., Bonoli, F., Cacciari, C., Djorgovski, S., Federici, L., Ferraro, F.R., Parmeggiani, G., Weir, N., & Zavatti, F. 1994, *A&A*, 284, 349
- Grillmair, C.J., Ajhar, E.A., Faber, S.M., Baum, W.A., Holtzman, J.A., Lauer, T.R., Lynds, C.R., & O'Neil, E.J. Jr. 1996, *AJ*, 111, 2293
- Huchra, J. 1993, in *ASP Conf. Ser.*, Vol. 48, *The Globular Cluster – Galaxy Connection*, G. Smith & J. Brodie (San Francisco: ASP), 420
- Huchra, J., Brodie, J.P., & Kent, S.M. 1991, *ApJ*, 370, 495
- King, I.R. 1966, *AJ*, 71, 64
- Meylan, G., & Mayor, M. 1986, *A&A*, 166, 122
- Osterbrock, D.E., Fulbright, J.P., Martel, A.R., Keane, M.J., Trager, S.C., & Basri, G. 1996, *PASP*, 108, 277
- Paturel, G., & Garnier, R. 1992, *A&A*, 254, 93
- Peterson, C.J., & King, I.R. 1975, *AJ*, 80, 427
- Peterson, R. 1988, in *Dynamique of Dense Stellar System*, ed. D. Merritt (Cambridge: Cambridge University Press), 161
- Pryor, C., & Melan, G. 1993, in *ASP Conf. Ser.*, Vol. 50, *Structure and Dynamics of Globular Clusters*, S. Djorgovski & G. Melan (San Francisco: ASP), 357
- Queloz, D., Dubath, P., & Pasquini, L. 1995, *A&A*, 300, 310
- Sargent, W.L., Kowal, C.T., Hartwick, F.D.A., & van den Bergh, S. 1977, *AJ*, 82, 947
- Spitzer, L. 1987, *Dynamical Evolution of Globular Clusters*, Princeton University Press, Princeton.
- Tripicco, M. 1993, in *ASP Conf. Ser.*, Vol. 48, *The Globular Cluster – Galaxy Connection*, G. Smith & J. Brodie (San Francisco: ASP), 432
- van den Bergh, S. 1994, *AJ*, 108, 2145
- Vogt, S. 1987, *PASP*, 99, 1214

*Note added in proof.* – As this paper was being accepted for publication, we became aware of a similar work by Djorgovski et al. (*ApJL*, in press). They derive velocity dispersions from Keck observations for a sample of 21 M31 globular clusters, which includes our 9 clusters. Their results are in good agreement with ours, e.g., the difference

in velocity dispersion values is always  $\leq 1.4 \text{ km s}^{-1}$  for all clusters. They point out an interesting trend between the ratio mass-to-luminosity in the K band and the cluster metallicity, which has not been observed before.